Open Research Online

Selecting suitable image dimensions for scanning probe microscopy

Journal Item

For guidance on citations see FAQs.

Version: Version of Record

oro.open.ac.uk
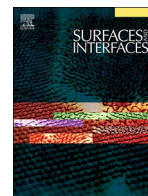
Selecting suitable image dimensions for scanning probe microscopy

James Bowen[a,*], David Cheneler[b]

[a] *School of Engineering and Innovation, The Open University, Walton Hall, Milton Keynes, MK7 6AA, UK*
[b] *Engineering Department, Lancaster University, Bailrigg, Lancaster, LA1 4YR, UK*

ABSTRACT

The use of scanning probe microscopy to acquire topographical information from surfaces with nanoscale features is now a common occurrence in scientific and engineering research. Image sizes can be orders of magnitude greater than the height of the features being analysed, and there is often a trade-off between image quality and acquisition time. This work investigates a commonly encountered problem in nanometrology - how to choose a scan size which is representative of the entire sample. The topographies of a variety of samples are investigated, including metals, polymers, and thin films.

1. Introduction

Surface metrology can be defined as the measurement of the deviations of a workpiece from its intended shape [1]. This include features such as deviations from roundness, straightness, flatness, cylindricity, and other descriptors of specimen shape. Surface topography measurement also detects the marks left on a specimen in trying to achieve the shape, such as those created by machining or polishing. Surface metrology is also highly relevant to nanotechnology and micro/nanofabrication, for example assessing the structure of thin films manufactured using vapour deposition [2-4], or using focused ion beam to etch surfaces [5–6]. Researchers in these fields represent a range of scientific and engineering disciplines, and hence may be unfamiliar with the complexities of measuring surface topography. It would be helpful if a simple set of rules or guidance could be established regarding topography measurement

The development of the scanning probe microscope, particularly the scanning tunnelling microscope (STM) [7] and the atomic force microscope (AFM) [8], revolutionised the ability to acquire three-dimensional topographical information. These techniques are now well-established as 'go-to' analytical tools when dealing with nanomaterials and nano-engineered surfaces. The versatility of AFM for imaging both conductive and insulating materials means it is particularly popular. Researchers have sought to capture the effect of scanning parameters such as scan speed [9], cantilever dynamics [10], tip size [11], and the choice of medium in which scanning is performed, e.g. liquid environment [12–13]. For example, Westra and Thomson investigated how the finite size of the AFM tip influenced surface profiles [14]. Vertical measures were found to be relatively insensitive to increasing

tip size. In contrast, lateral measures became increasingly distorted as tip size increased.

The 1-dimensional average roughness, R_a, of a surface is defined as ``arithmetic mean deviation from the centre line through the profile'' and is expressed mathematically by Eq. (1), in which n is the number of pixels in the image, and y_i is the deviation from the centre line for each pixel.

$$R_a = \frac{1}{n} \sum_{i=1}^{n} |y_i| \tag{1}$$

The aim of this work was to address the question "does there exist an optimal range of image sizes for the measurement of nanoscale surface roughness?" Characterisation of the surface topography of a selection of polished, machined, deposited and cast surfaces was performed using atomic force microscopy. Image sizes in the range 0.1–100 μm were employed, and the average roughness was calculated for each image.

2. Experimental

2.1. Sample preparation

Samples were immobilised onto steel specimen disks (Agar Scientific, UK) using cyanoacrylate adhesive (Loctite, UK) prior to measurement. If required, samples were trimmed to dimensions of 30 mm × 30 mm or smaller. The samples prepared were

(i) Al_2O_3 disc (Agar Scientific, UK)
(ii) polished steel disc (Agar Scientific, UK)

* Corresponding author.
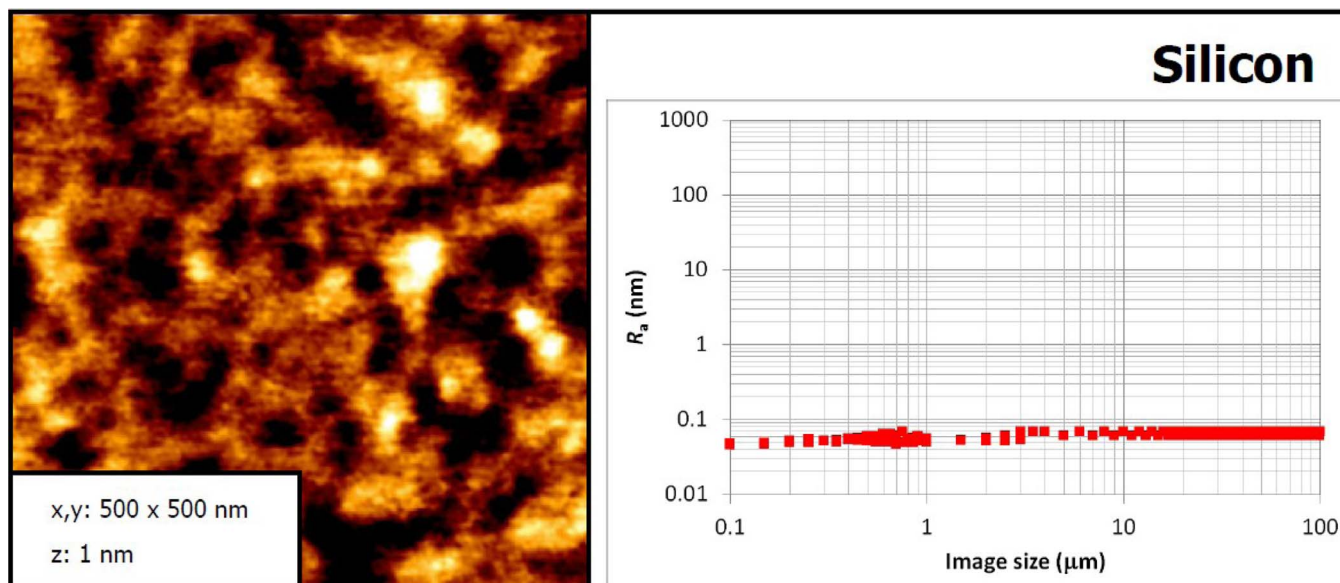 *E-mail address:* james.bowen@open.ac.uk (J. Bowen).

Fig. 1. AFM image ($x,y = 500$ nm; $z = 1$ nm) and R_a as a function of image size for Si(100).

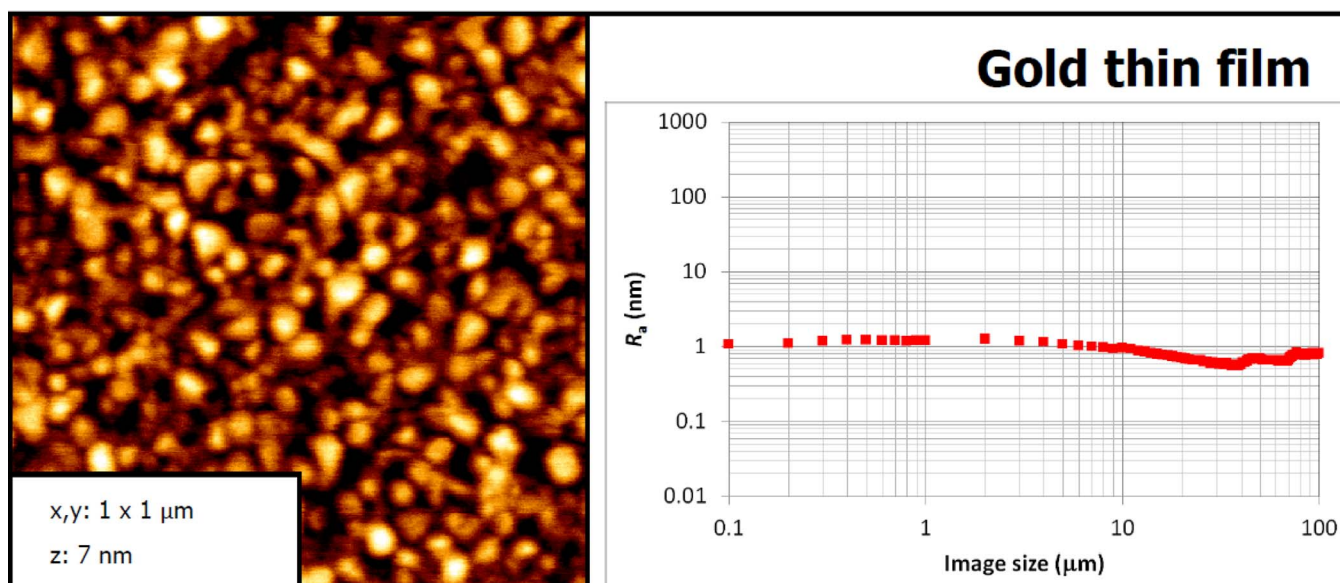Fig. 2. AFM image ($x,y = 1$ μm; $z = 7$ nm) and R_a as a function of image size for 30 nm Au film.

(iii) poly(methyl methacrylate) tile (in-house supply)
(iv) poly(styrene) Petri dish (BD Falcon, UK)
(v) poly(tetrafluoroethylene) sheet (Altec, UK)
(vi) CaF_2 window (Crystran, UK)
(vii) Si(100) wafer (IDB Technologies, UK)
(viii) 30 nm Au film thermally evaporated onto Si wafer (Georg Albert PVD, Germany)
(ix) 100 nm CF_xO_y film deposited onto Si wafer using plasma polymerisation, see Cheneler et al. [15] for further details.

2.2. Characterisation using AFM

Surface topographies were measured within square scan windows, with equal *x*- and *y*-dimensions. The length of the *x*-dimension is hereafter referred to as the Image Size, *s*. The Image Size was varied in the range 0.1 μm–100 μm. A line pixel density, *p*, of 512 pixels was employed throughout; this means that images were composed of a square array of pixels measuring 512×512.

Images were acquired using a NanoWizard II AFM (JPK Instruments, UK) operating in Contact Mode at a temperature of 18 °C and a relative humidity of <40%. Rectangular pyramidal-tipped Si cantilevers (CSC17/noAl, MikroMasch, Estonia) with a nominal tip diameter of <10 nm were employed. Samples analysed using the AFM were held in place using a custom-built magnetic sample stage. 1-dimensional image analysis was performed using JPK Data Processing software (JPK Instruments, UK), while 2-dimensional image analysis was performed using Scanning Probe Image Processor software (Image Metrology, Denmark). Plane correction was performed using linewise levelling.
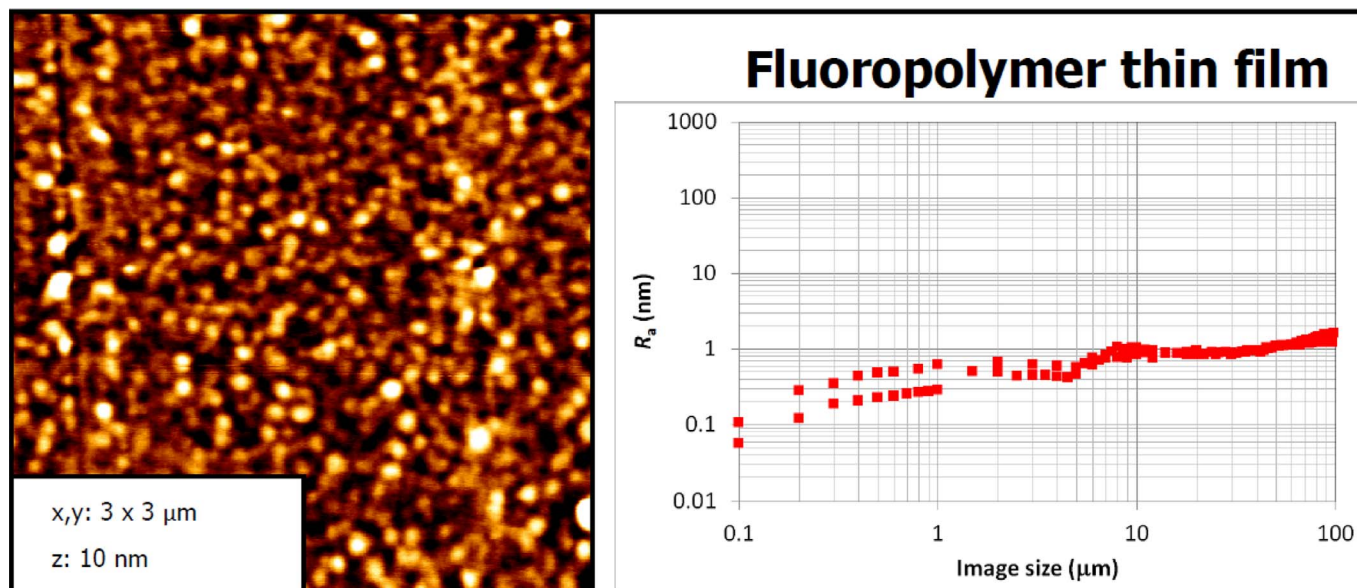
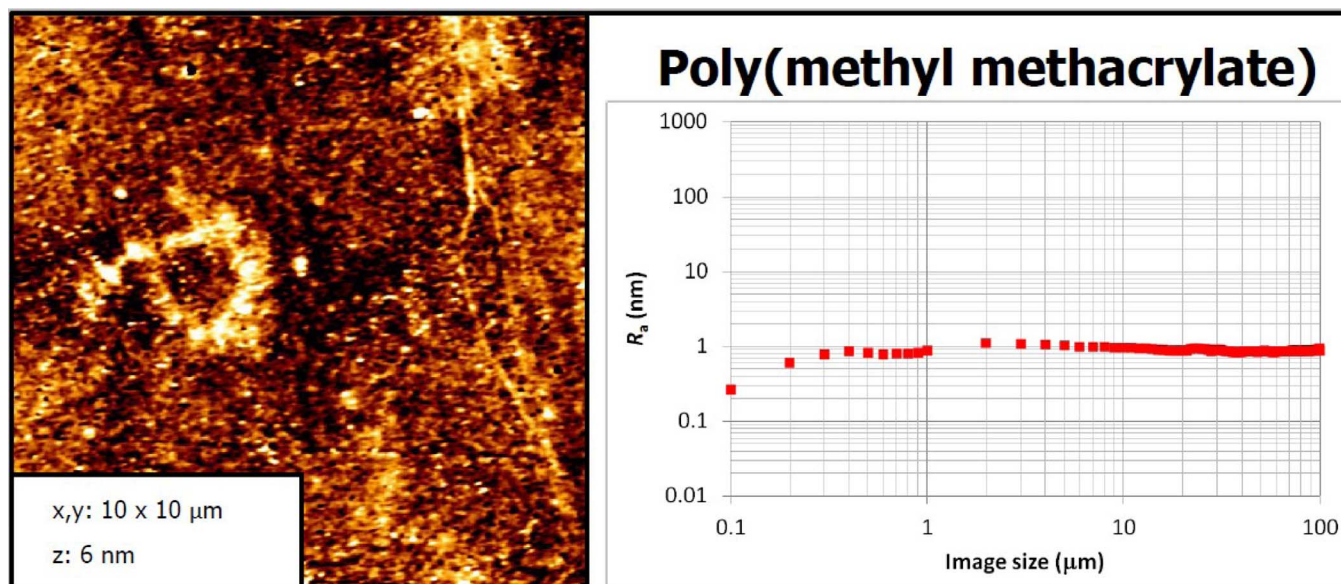**Fig. 3.** AFM image (x,y = 3 µm; z = 10 nm) and R_a as a function of image size for 100 nm CF$_x$O$_y$ film.

Fig. 4. AFM image (x,y = 10 µm; z = 6 nm) and R_a as a function of image size for poly(methyl methacrylate).

3. Results

The results are presented in order of increasing maximum surface roughness. Inset in each figure are the x,y dimensions of the image, as well as the image height scale or z-scale, which is hereafter referred to as z. Each figure shows the roughness, R_a, of the surface as a function of Image Size, s.

3.1. Silicon wafer

Fig. 1 shows that the surface of a Si wafer exhibits R_a < 0.1 nm across the AFM Image Size range 0.1–100 µm. Multiple locations were scanned on the sample, and these data points overlap strongly. The lateral dimensions of the surface features are on the order $f \sim 50$ nm.

3.2. Thermally evaporated Au thin film

Fig. 2 shows that the surface of a thermally evaporated Au thin film, deposited onto a silicon wafer, exhibits $R_a \sim 1$ nm across the AFM Image Size range 0.1–100 µm. The lateral dimensions of the surface features, clusters of Au atoms, are on the order $f \sim 40$–80 nm. In contrast with the Si wafer (Fig. 1) however, there exists a maximum R_a, which occurs at $s \sim 2$ µm. For image sizes in the range 2 µm $< s <$ 40 µm there is a gradual decrease in R_a. At $s > 40$ µm the R_a increases once again, but does not exceed the maximum R_a measured at $s \sim 2$ µm.

3.3. Plasma polymerised fluoropolymer thin film

Fig. 3 shows that the surface of a plasma polymerised CF$_x$O$_y$ thin film, deposited onto a silicon wafer, exhibits R_a < 2 nm across the AFM
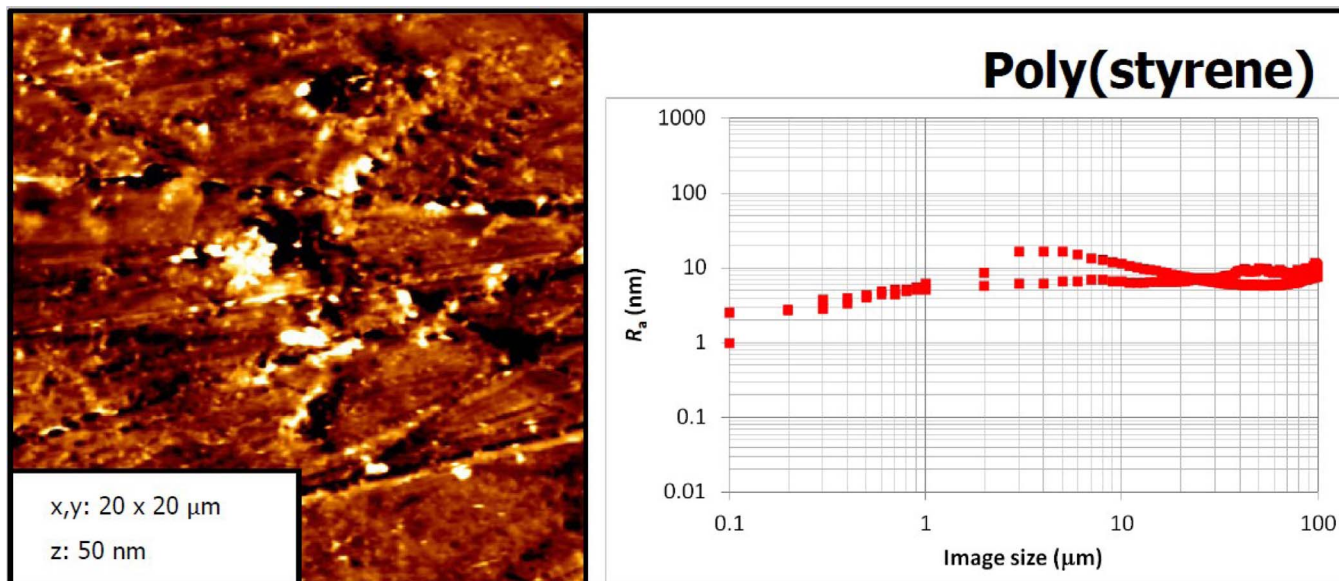
Fig. 5. AFM image (x,y = 20 μm; z = 50 nm) and R_a as a function of image size for poly(styrene).

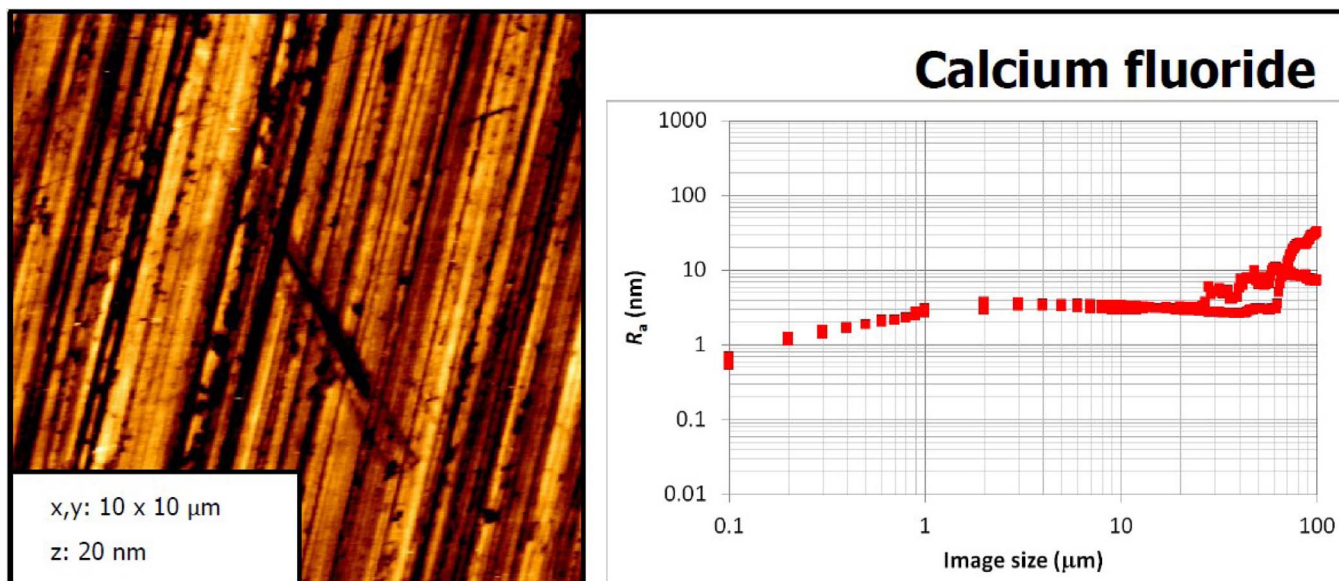**Fig. 6.** AFM image (x,y = 10 μm; z = 20 nm) and R_a as a function of image size for CaF$_2$.

Image Size range 0.1–100 μm. Multiple locations were scanned on the sample, and these data points overlap closely for s > 5 μm. The lateral dimensions of the surface features, fluoropolymer `blobs', are on the order f ~ 100 nm. Similarly to the Au thin film (Fig. 2) the R_a peaks at s ~ 2 μm. R_a then decreases slightly for $2 μ < s < 5$ μm, before gradually increasing up to s = 100 μm, albeit with a slight decrease in the range 10 μm < s < 30 μm.

3.4. Poly(methyl methacrylate) tile

Fig. 4 shows that the surface of a poly(methyl methacrylate) tile exhibits R_a ~ 1 nm across the AFM Image Size range 0.4–100 μm. The lateral dimensions of the surface features varies in the approximate range 30 < f < 250 nm. For this surface there also exists a maximum

R_a, which once again occurs at s ~ 2 μm. For image sizes in the range 3 μm < s < 20 μm there is a gradual decrease in R_a. For s > 20 μm the R_a remains approximately constant around 1 nm.

3.5. Poly(styrene) petri dish

Fig. 5 shows that the surface of a poly(styrene) Petri dish exhibits roughness in the range 1 nm < R_a < 20 nm across the AFM Image Size range 0.1–100 μm. Multiple locations were scanned on the sample. The lateral dimensions of the surface features are difficult to characterise using a single parameter, due to the complex topography presented. For this surface there also exists a maximum R_a, around 20 nm, which occurs at s ~ 4 μm. For image sizes in the range $4 < s \leq 100$ μm the surface roughness remains in the range 6 nm < R_a < 20 nm.
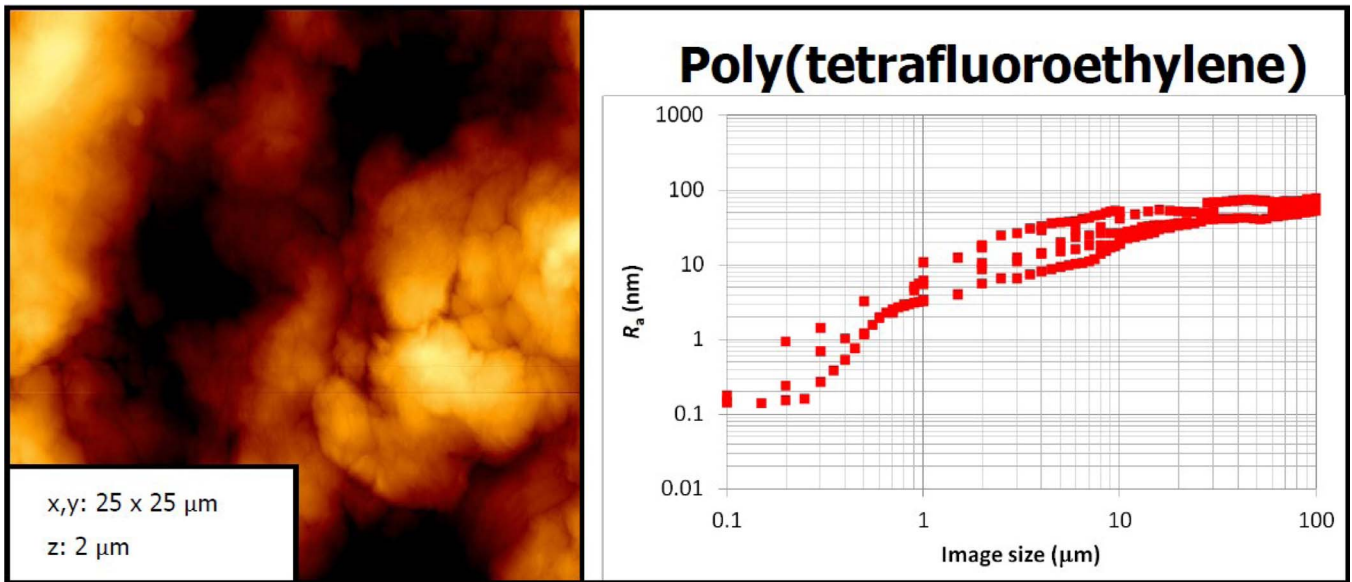
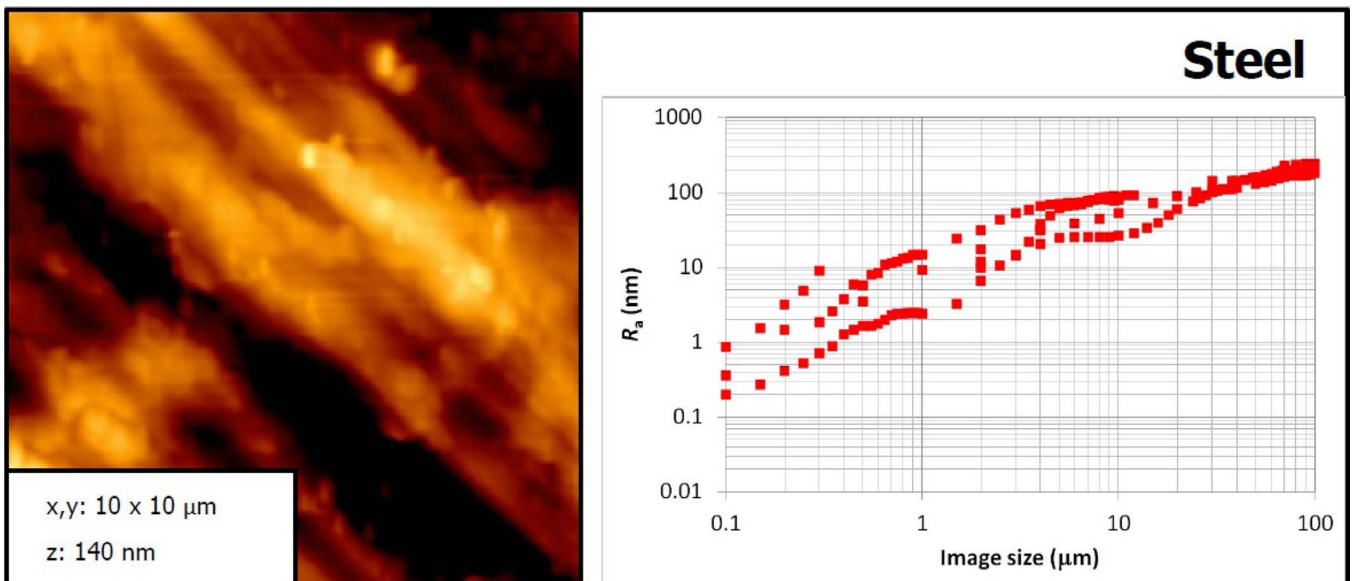**Fig. 7.** AFM image (x,y = 25 µm; z = 2 µm) and R_a as a function of image size for poly(tetrafluoroethylene).

Fig. 8. AFM image (x,y = 10 µm; z = 140 nm) and R_a as a function of image size for steel.

3.6. Calcium fluoride window

Fig. 6 shows that the surface of a calcium fluoride window exhibits roughness in the range 0.5 nm $< R_a <$ 3 nm across the AFM Image Size range 0.1 $< s \leq$ 1 µm. The surface roughness remains in the range 2–3 nm for 1 µm $< s \leq$ 20 µm. Multiple locations were scanned on the sample, which gave rise to a variety of roughness profiles for $s >$ 20 µm. It is not possible to characterise the lateral dimensions of the complex surface topography using a single parameter. However, there was a dominant direction of polishing marks visible when $s <$ 30 µm. The lateral dimensions of these surface features lies in the approximate range 75 nm $< f <$ 150 nm. In all instances, R_a increased significantly for $s >$ 20 µm, approaching a maximum of $R_a \sim$ 40 nm at $s =$ 100 µm.

3.7. Poly(tetrafluoroethylene) sheet

Fig. 7 shows that the surface of a poly(tetrafluoroethylene) sheet exhibits increasing roughness in the range 0.15 $< R_a <$ 90 nm across the AFM Image Size range 0.1–100 µm. Multiple locations were scanned on the sample, which gave rise to a variety of roughness profiles. The surface topography was not suitable for characterisation using a single parameter for the lateral structure. For $s >$ 40 µm, the surface roughness presented was usually in the range 40 nm $< R_a <$ 90 nm.

3.8. Steel disc

Fig. 8 shows that the surface of a steel disc exhibits increasing roughness in the range 0.2 nm $< R_a <$ 250 nm across the AFM Image

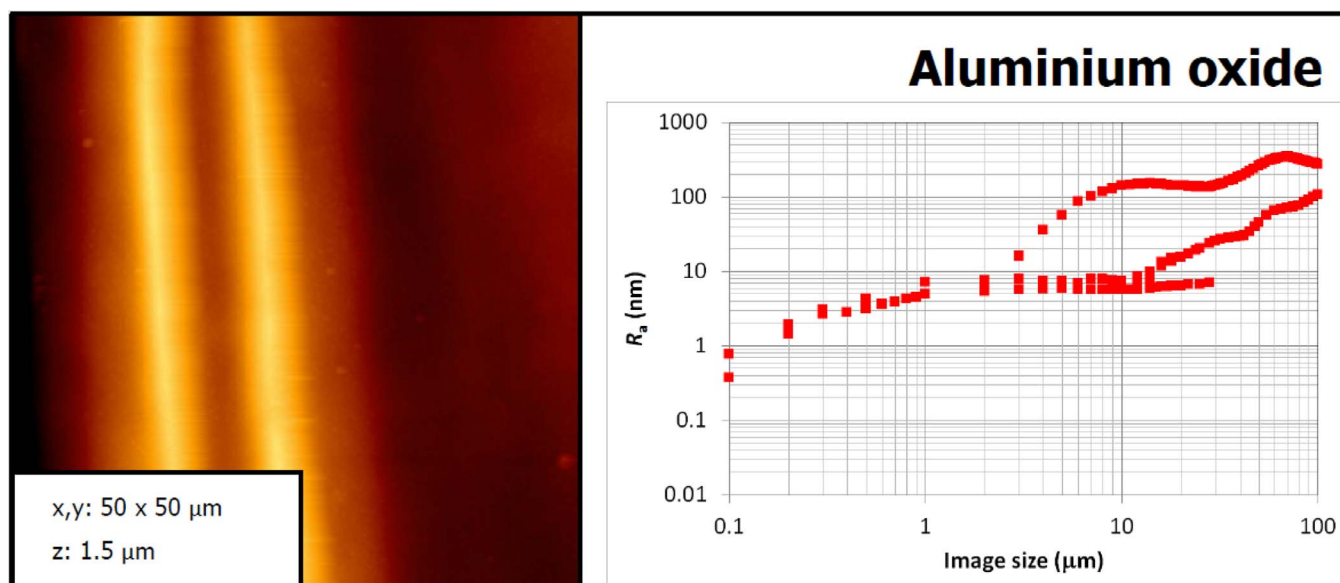**Fig. 9.** AFM image ($x,y = 1\,\mu m$; $z = 1.5\,\mu m$) and R_a as a function of image size for Al_2O_3.
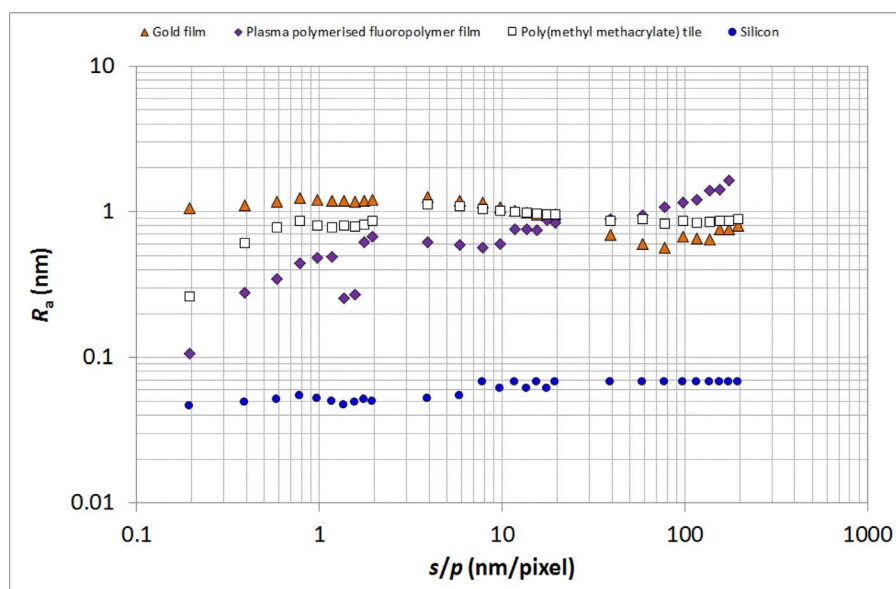

Fig. 10. Relationship between the pixel size, $\frac{s}{p}$, and the average roughness, R_a, for the poly(methyl methacrylate) tile, Si(100) wafer, 30 nm Au film, and 100 nm CF_xO_y film.

Size range 0.1–100 μm. Multiple locations were scanned on the sample, which gave rise to a variety of roughness profiles. For $s > 30\,\mu m$, the surface roughness presented was greater than 100 nm, increasing to $R_a = 250\,nm$ at $s > 100\,\mu m$.

3.9. Aluminium oxide disc

Fig. 9 shows that the surface of an aluminium oxide disc exhibits increasing roughness in the range $0.4\,nm < R_a < 400\,nm$ across the AFM Image Size range 0.1–100 μm. Multiple locations were scanned on the sample, which gave rise to a variety of roughness profiles. For $s \leq 2\,\mu m$, the surface roughness presented was less than 8 nm, increasing to $R_a \sim 160\,nm$ at $s > 10\,\mu m$ for one sample. Other samples did not exhibit such a strong dependence on the location on which imaging centred.

4. Discussion

4.1. Effect of pixel density

The samples can be divided into two categories: (a) those with surfaces which can be defined by a single lateral dimension; and (b) those with surfaces which are too complex to define using a single parameter. For the range of Image Sizes used in this work, $0.1\,\mu m \leq s \leq 100\,\mu m$, only the poly(methyl methacrylate) tile, Si(100) wafer, 30 nm Au film, and 100 nm CF_xO_y film fall into category (a). The CaF_2 window, Al_2O_3 disc, poly(styrene) Petri dish, and poly(tetrafluoroethylene) sheet, and steel disc all fall into category (b).

For samples in category (a) there appears to be a critical image size at which the measured surface roughness reaches an apparent maximum. Such behaviour is an artifact of there being insufficient pixel
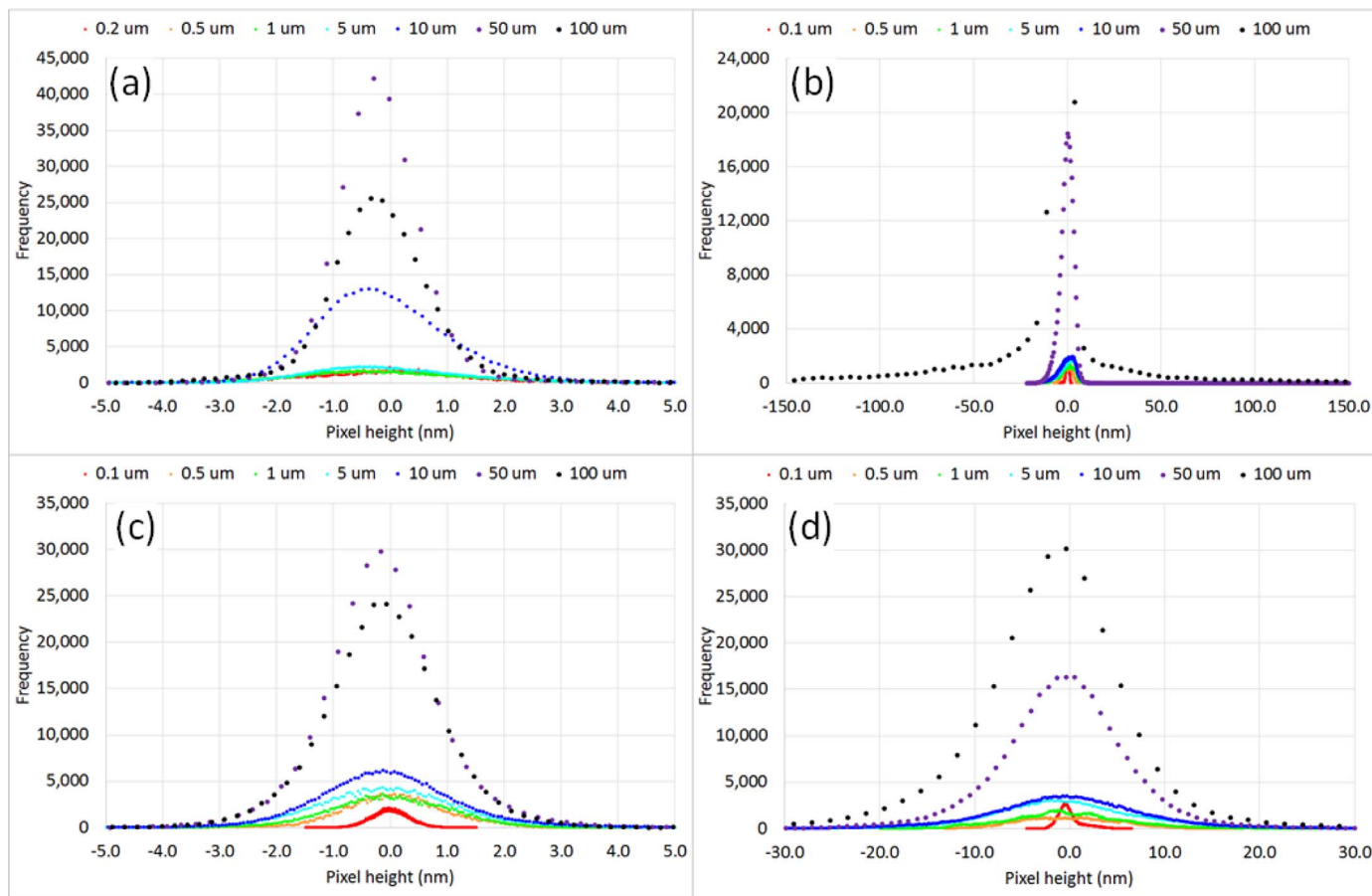
Fig. 11. Pixel height distributions as a function of image size for (a) Au, (b) CaF$_2$, (c) poly(methyl methacrylate), (d) poly(styrene).

density available with which to construct the smallest surface features. As the image size increases further, the measured surface roughness decreases slightly, contrary to expectations. If each image size successfully captured the 'character' of the surface, there should be no decrease in roughness, unless a region of different topography was encountered as the scan area increased.

Using the data for the poly(methyl methacrylate) tile, Si(100) wafer, 30 nm Au film, and 100 nm CF$_x$O$_y$ film, Fig. 10 is a plot of the pixel size, $\frac{s}{p}$, versus R_a. The maximum R_a occurs in the range $2 < \frac{s}{p} < 20$, with the exception of the 100 nm CF$_x$O$_y$ film, which exhibits a gradual increase in R_a from $\frac{s}{p} \sim 80$.

So what advice could be given when attempting to measure highly polished surfaces, or films with nanoscale features and which conform strongly to the underlying substrate? Images should be generated using high pixel densities relative to the dimensions of the smallest lateral features present on a surface. i.e. low $\frac{s}{p}$. This strategy should provide a high quality of scanning across the surface topography. For the surfaces investigated in this work, values of $\frac{s}{p} < 20$ yielded values of R_a which did not appear to be compromised by inappropriate choice of scanning parameters relative to the dimensions of surface features.

With regards to the samples in category (b), these surfaces exhibited hierarchies of features, resulting in surface roughness profiles which tended to yield increasing values of R_a with increasing values of s. Further, scanning multiple regions of the same sample gave little overlap between roughness curves, particularly for $s > 1$ μm. Practical advice which could be applied when measuring samples such as these

must include (i) scan multiple locations, (ii) scan multiple image sizes, (iii) consider acquiring data using a measurement technique which operates at lateral length scales greater than AFM, such as profilometry.

4.2. Choice of roughness descriptors

Four samples were chosen for an exploration of additional roughness descriptors. The samples were (i) 30 nm Au film, (ii) CaF$_2$ window, (iii) poly(methyl methacrylate) tile, and (iv) poly(styrene) Petri dish. The additional descriptors are as follows.

The 1-dimensional root-mean-square roughness, R_q, Eq. (2):

$$R_q = \left(\frac{1}{n} \sum_{i=1}^{n} y_i^2 \right)^{0.5}$$

(2)

The 1-dimensional height range, R_z, Eq. (3):

$$R_z = \max_i y_i + \min_i y_i$$

(3)

The skewness of the pixel height distribution, S_{sk}, Eq. (4):

$$S_{sk} = \frac{1}{nR_q^3} \sum_{i=1}^{n} y_i^3$$

(4)

The kurtosis of the pixel height distribution, S_{ku}, Eq. (5):
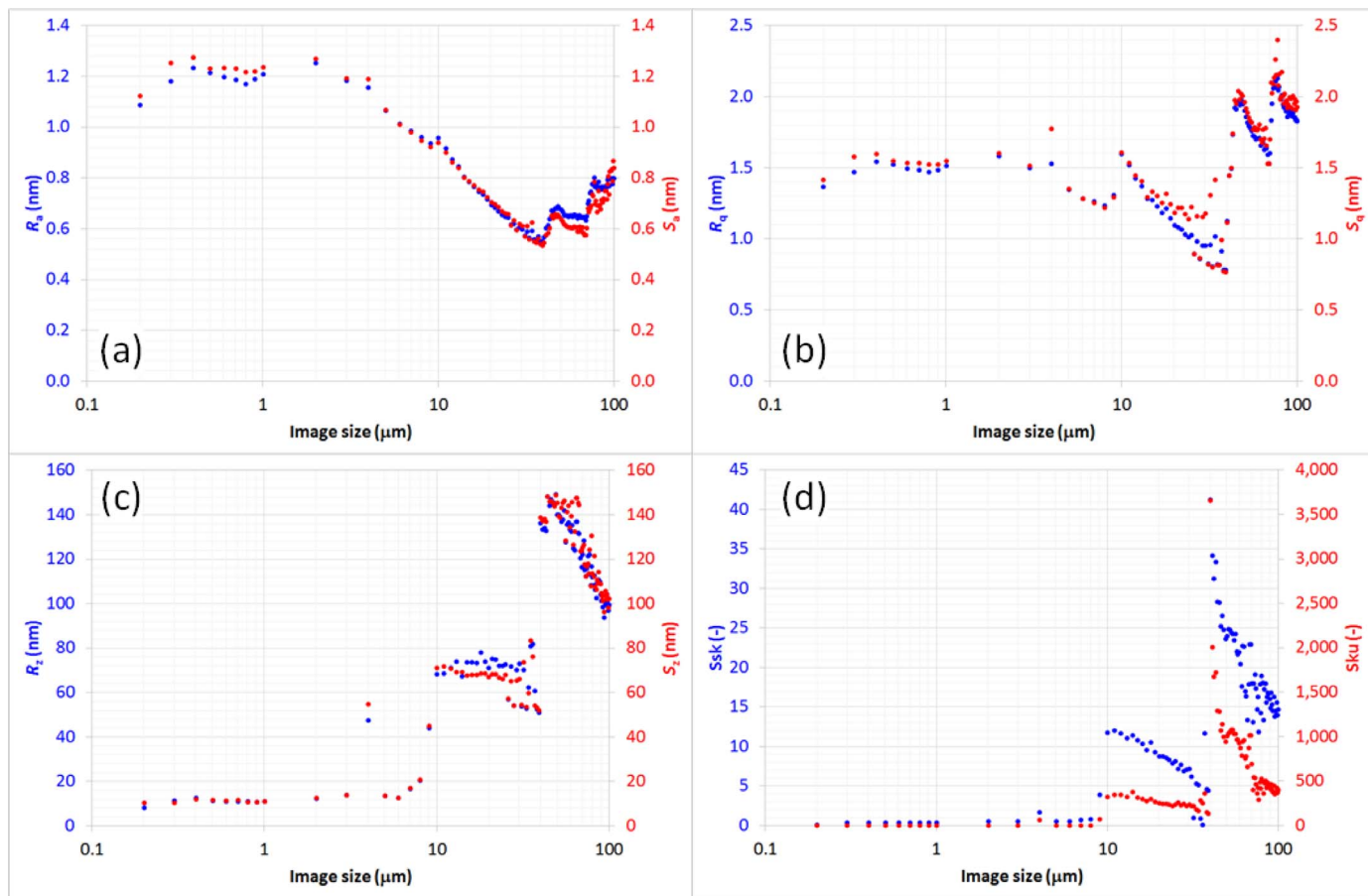
$$S_{ku} = \frac{1}{nR_q^4} \sum_{i=1}^{n} y_i^4$$

(5)

Fig. 12. Roughness descriptors as a function of image size for Au: (a) R_a vs S_a, (b) R_q vs S_q, (c) R_z vs S_z, (d) S_{sk} vs S_{ku}.

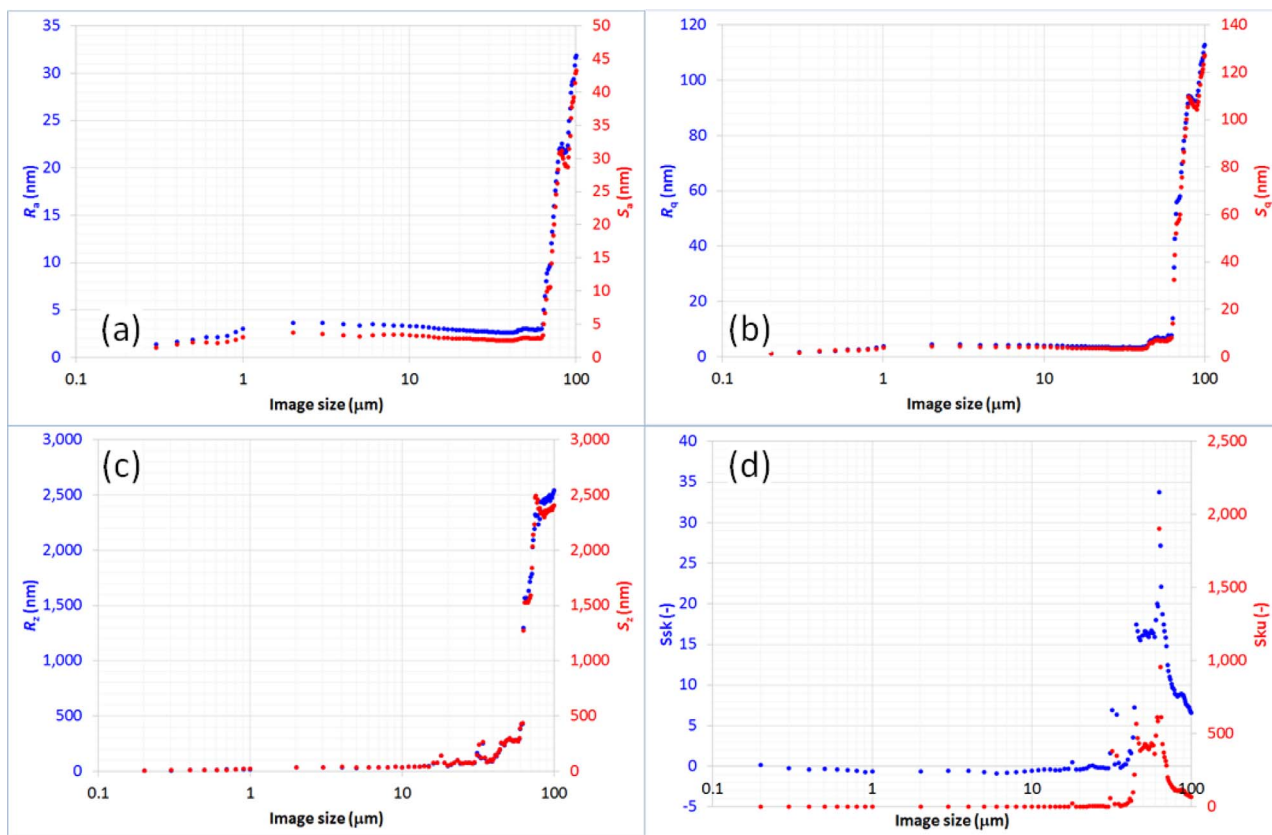**Fig. 13.** Roughness descriptors as a function of image size for CaF$_2$: (a) R_a vs S_a, (b) R_q vs S_q, (c) R_z vs S_z, (d) S_{sk} vs S_{ku}.

Fig. 14. Roughness descriptors as a function of image size for poly(methyl methacrylate): (a) R_a vs S_a, (b) R_q vs S_q, (c) R_z vs S_z, (d) S_{sk} vs S_{ku}.
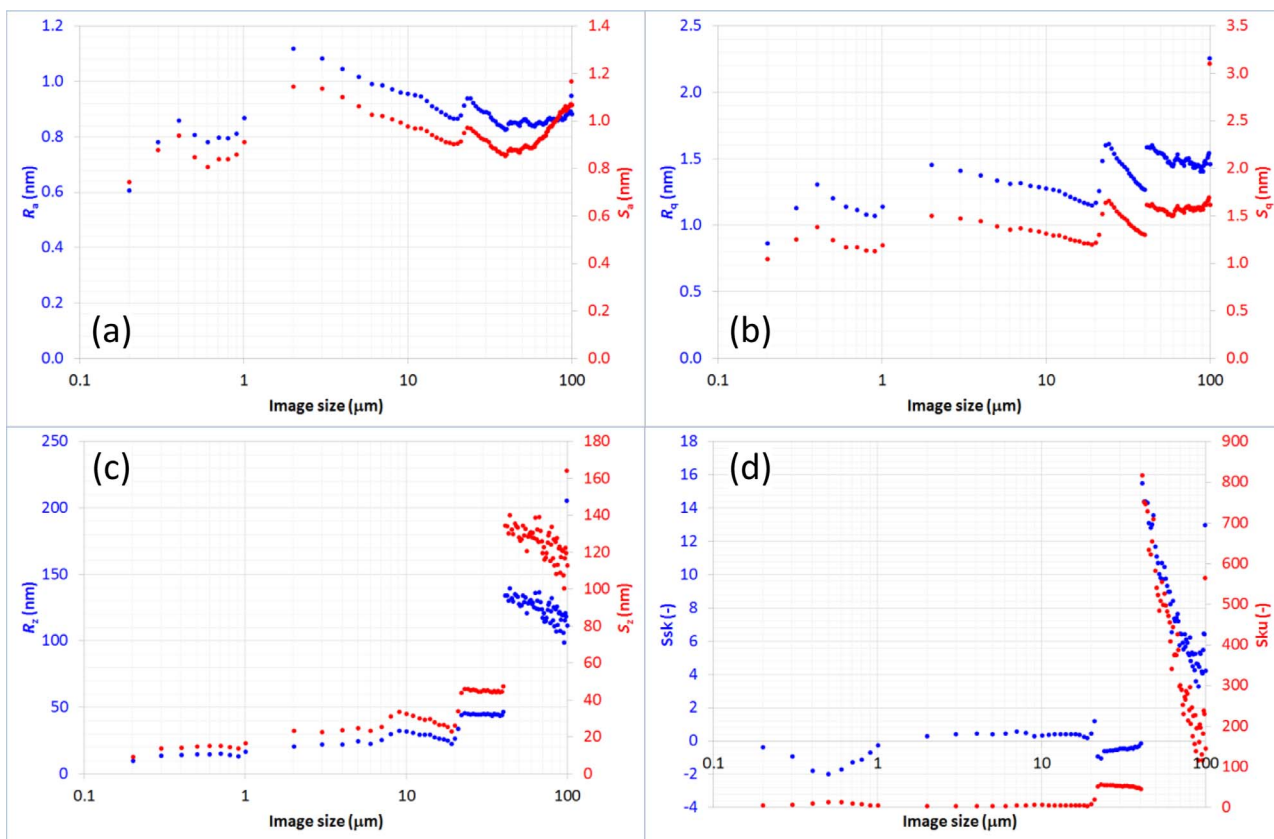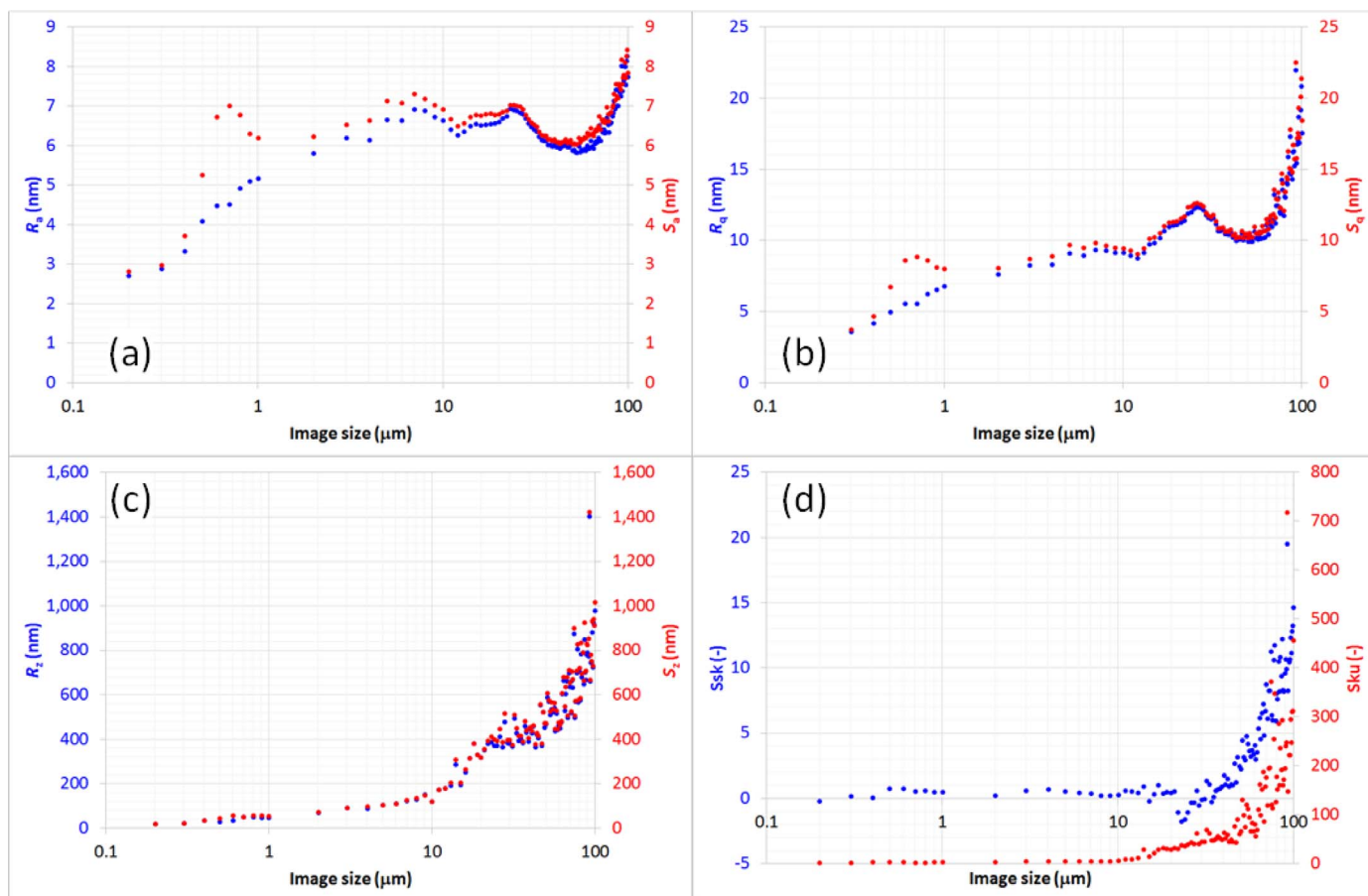
Fig. 15. Roughness descriptors as a function of image size for poly(styrene): (a) R_a vs S_a, (b) R_q vs S_q, (c) R_z vs S_z, (d) S_{sk} vs S_{ku}.

Further, the 2-dimensional variants of R_a, R_q, and R_z were investigated; these are referred to as S_a, S_q, and S_z respectively.

The pixel height distributions for the four samples are shown in Fig. 11. For clarity of presentation, histograms from regularly spaced image sizes are shown. The distribution of pixel heights is approximately symmetric for Au, poly(methyl methacrylate), and poly(styrene), whereas for CaF_2 the distribution displays asymmetry at all image sizes.

Figs. 12–15 show the descriptor comparisons for Au, CaF_2, poly(methyl methacrylate), and poly(styrene) respectively. For each sample, each pair of 1-dimensional and 2-dimensional descriptors follows the same trend as a function of image size. There is little difference in value between each descriptor pair for Au, CaF_2, and poly(styrene). The results for poly(methyl methacrylate) are a notable exception. The use of these descriptors does not reveal trends as a function of image size which are not shown in the average roughness plots, Figs. 1–9.

5. Conclusion

This work sought to investigate the influence of the choice of analysis conditions when measuring surface topography using atomic force microscopy. In particular, the importance of pixel density and image dimensions. The topography of nine samples were measured using square images of x, y-dimensions in the range 0.1–100 μm. The average roughness of each image was calculated and plotted as a function of image size. Where possible, the approximate dimension of the smallest surface feature was also defined.

Pixel sizes smaller than 20 nm appeared to be optimal for the characterisation of surfaces with nanoscale topography. Increasing the pixel density of an image should afford the possibility of imaging larger areas without compromising feature resolution. Surfaces which exhibit a hierarchy of topographies should be treated cautiously, and may not be suitable for nanoscale analysis unless well-defined regions free from machining marks are highlighted and analysed in isolation.

The use of descriptors such as root-mean-square roughness, height range, skewness and kurtosis does not reveal trends as a function of image size, which are not captured by the average roughness. Further, a comparison of 1-dimensional and 2-dimensional roughness descriptors did not display a noticeable deviation in the recorded trends.

References

[1] D.J. Whitehouse, Handbook of Surface and Nanometrology, second ed., CRC Press (Boca Raton), 2011.
[2] K. Reichelt, H.O. Lutz, Hetero-epitaxial growth of vacuum evaporated silver and gold, J. Cryst. Growth (1971) 103–107.
[3] C.E.D. Chidsey, D.N. Loiacono, T. Sleator, S. Nakahara, STM study of the surface morphology of gold on mica, Surf. Sci. (1988) 45–66.
[4] J.A. DeRose, T. Thundat, L.A. Nagahara, S.M. Lindsay, Gold grown epitaxially on mica: conditions for large area flat faces, Surf. Sci. 256 (1991) 102–108.
[5] A. Sabouri, C.J. Anthony, J. Bowen, V. Vishnyakov, P.D. Prewett, The effects of dwell time on focused ion beam machining of silicon, Microelectron. Eng 121 (2014) 24–26.
[6] A. Sabouri, C.J. Anthony, P.D. Prewett, J. Bowen, H. Butt, Effects of current on early stages of focused ion beam nanomachining, Mater. Res. Exp. 2 (2015) 055005.
[7] G. Binnig, H. Rohrer, C. Gerber, E. Weibel, Surface studies by scanning tunneling microscopy, Phys. Rev. Lett. 49 (1982) 57–61.
[8] G. Binnig, C.F. Quate, C. Gerber, Atomic force microscope, Phys. Rev. Lett. 56 (1986) 930–933.
[9] H-J. Butt, P. Siedle, K. Seifert, K. Fendler, T. Seeger, E. Bamberg, A.L. Weisenhorn, K. Goldie, A. Engel, Scan speed limit in atomic force microscopy, J. Microsc. 169 (1993) 75–84.
[10] A. Kühle, A.H. Sørensen, J.B. Zandbergen, J. Bohr, Contrast artifacts in tapping tip atomic force microscopy, Appl. Phys. A 66 (1998) S329–S332.
[11] D.L. Sedin, K.L. Rowlen, Influence of tip size on AFM roughness measurements, Appl. Surf. Sci. 182 (2001) 40–48.
[12] E.F. de Souza, R.A. Douglas, O. Teschke, Atomic force microscopic imaging in liquids: effects of the film compressed between the substrate and the tip, Langmuir 13 (1997) 6012–6017.
[13] F. Ohnesorge, Towards atomic resolution non-contact dynamic force microscopy in a liquid, Surf. Interface Anal. 27 (1999) 379–385.
[14] K.L. Westra, D.J. Thomson, Effect of tip shape on surface roughness measurements from atomic force microscopy images of thin films, J. Vac. Sci. Technol. B 13 (1995) 344–349.
[15] D. Cheneler, J. Bowen, S.D. Evans, M. Górzny, M.J. Adams, M.C.L. Ward, Characteristics and durability of fluoropolymer thin films, Polym. Degrad. Stabil. 96 (2011) 561–565.